

Hypernuclear weak decay of ${}_{\Lambda}^{12}\text{C}$ and ${}_{\Lambda}^{11}\text{B}$

H. Noumi,* S. Ajimura, H. Ejiri,† A. Higashi,‡ and T. Kishimoto
Department of Physics, Faculty of Science, Osaka University, Toyonaka, Osaka 560, Japan

D. R. Gill, L. Lee, and A. Olin
TRIUMF, Vancouver, British Columbia, Canada V6T 2A3

T. Fukuda and O. Hashimoto
Institute for Nuclear Study, University of Tokyo, Tanashi, Tokyo 188, Japan
 (Received 21 April 1995)

The branching ratios of negative pions and protons due to the weak decays of ${}_{\Lambda}^{12}\text{C}$ and ${}_{\Lambda}^{11}\text{B}$ hypernuclei were measured. The negative pionic decay rates (Γ_{π^-}), proton-induced nonmesonic decay rates (Γ_p), total nonmesonic decay rates (Γ_{nm}), and ratios of the $\Lambda n \rightarrow nn$ process to the $\Lambda p \rightarrow pn$ process (Γ_n/Γ_p) were derived from the present measurements combined with previous studies on the mesonic π^0 and total decay rates. The measured Γ_{π^-} shows that Pauli blocking is less effective than expected due to pion distortion. We found that Γ_{nm} is nearly equal to unity in units of the free-space Λ -decay width. The present results also indicate that Γ_n is almost twice that of Γ_p . This is in disagreement with calculations based on meson-exchange models in which Γ_n is strongly suppressed.

PACS number(s): 21.80.+a, 25.80.Hp

I. INTRODUCTION

In single Λ hypernuclei a Λ hyperon is free from the Pauli exclusion principle which governs nucleons because it has a different quantum number, strangeness ($S \neq 0$). Consequently, the Λ can occupy any orbital in the hypernucleus. In general, the excited hypernucleus is stable against Λ emission and decays into the ground state by emitting nucleons and/or γ rays. It eventually decays by weak processes. The decay properties reflect the dynamics of the hyperon and the nucleons in the hypernucleus. We can learn through studies of hypernuclear weak decays how real and/or virtual bosons propagate and how baryons and/or quarks correlate in the nuclear medium. However, experimental data on hypernuclear weak decays are limited, and there remain many questions. It is of particular importance to accumulate higher-quality data to constrain the various theoretical models put forth.

A hypernucleus decays in two predominant hadronic weak processes, which are characterized by the following elementary processes:

$$\text{M decay, } \Lambda \rightarrow p + \pi^-, n + \pi^0, \quad \Delta q \sim 100 \text{ MeV}/c, \quad (1)$$

$$\text{NM decay, } \Lambda + N \rightarrow p + n, n + n, \quad \Delta q \sim 400 \text{ MeV}/c. \quad (2)$$

*Present address: National Laboratory for High Energy Physics, Tsukuba, Ibaraki 305, Japan.

†Present address: Research Center for Nuclear Physics, Osaka University, Ibaraki, Osaka 567, Japan.

‡Present address: National Institute of Radiological Sciences, Inage-ku, Chiba 263, Japan.

Mesonic decay (M decay) is well known through studies of nonleptonic- Λ decays in free space. M decay can be used as a good tool to identify hypernuclei and to determine the spin of hypernuclei. M decay is suppressed in hypernuclei with $A \geq 7$ due to Pauli blocking effects because the momentum transfer, $\Delta q \sim 100 \text{ MeV}/c$, is much smaller than the Fermi momentum of $\sim 250 \text{ MeV}/c$. The suppression of the M decay rates ($\Gamma_{\pi^-}, \Gamma_{\pi^0}$) is reduced by the ΛN many-body interaction and by a distortion of the pion wave in the nuclear medium [1,2]. Systematic studies of the M decay rates are of interest.

Nonmesonic decay (NM decay) predominates in hypernuclei, except for light hypernuclei. It provides a unique opportunity to investigate the ΛN weak interaction since the transition $\Lambda N \rightarrow NN$ can take place only in the nucleus. The NM decay rates, Γ_p (proton-induced decay rate) and Γ_n (neutron-induced decay rate), are good observables through which the decay mechanism can be clarified. Until now, no theoretical calculations based on meson-exchange models can reproduce the experimental measurements on the NM decay rates, particularly on the ratio of Γ_n to Γ_p [3–5]. It has recently been suggested [6] that the discrepancy between theory and experiment may be explained by multinucleon-induced processes, such as $\Lambda NN \rightarrow NNN$, although this has not yet been established very well.

In recent years a series of counter experiments carried out at BNL measured a set of weak decay rates, the lifetime ($\tau = 1/\Gamma_{\text{tot}}$), and the partial rates (Γ_{π^-} , Γ_p , and Γ_n), in ${}_{\Lambda}^5\text{He}$, ${}_{\Lambda}^{11}\text{B}$, and ${}_{\Lambda}^{12}\text{C}$ produced via (K^-, π^-) reactions [7,8]. Before the BNL measurements the experimental data were limited to those from old emulsion and bubble-chamber experiments, where identification of hypernuclei was difficult, except for very light hyperfragments. The counter experiments improved the quality of data very much. However, only the lifetimes could be obtained for ${}_{\Lambda}^{11}\text{B}$ and ${}_{\Lambda}^{12}\text{C}$ because a large background from in-flight kaon decays contaminated the hy-

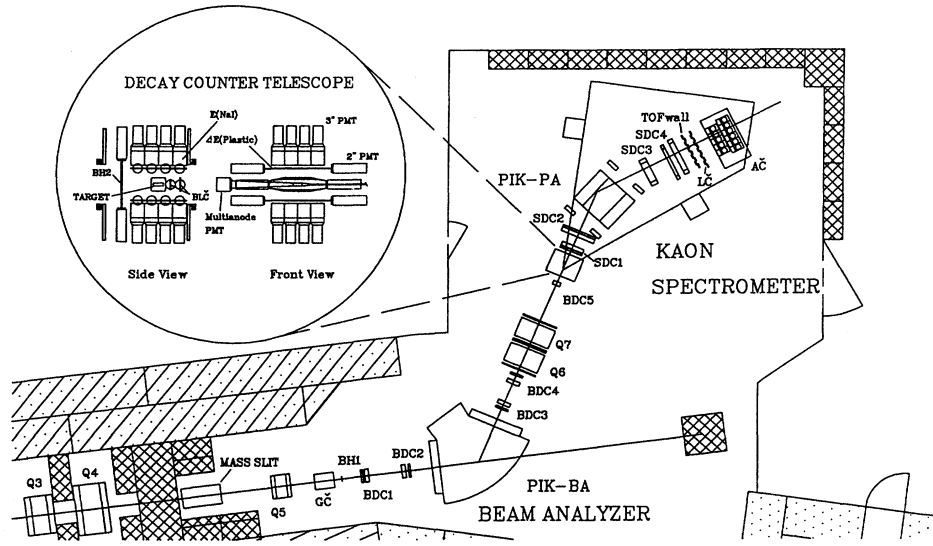


FIG. 1. Schematic view of the experimental setup. Counter telescopes for decay particles from hypernuclei were newly installed in the PIK spectrometer constructed for the previous experiment [12]. The pion beam was defined by counter hodoscopes BH1 and BH2. Positrons contaminated in the beam were rejected by a gas Čerenkov counter GC. The momenta of the pions were analyzed by the magnetic spectrometer (PIK-BA) and drift chambers (BDC1–BDC5). Differential lucite Čerenkov counters (BLČ's) were located behind an active scintillator target (TGT) to discard beam pions passing through, but not interacting with, the target. Scattered particles were triggered by a hodoscope TOF. Kaons were discriminated by two Čerenkov detectors, LC and AC. The momenta of the kaons were reconstructed by the magnetic spectrometer (PIK-PA) and drift chambers (SDC1–SDC4). The decay counter telescopes were set above and below the target. Each counter telescope set comprised an array of ΔE (plastic) and E (NaI) counters.

pernuclear excitation-energy spectrum. Therefore an improvement of this measurement is desired.

We recently carried out an experiment to study the polarizations and weak decays of hypernuclei produced via (π^+, K^+) reactions on ${}^{12}\text{C}$ at KEK (PS E160) [9]. In the present work we report on the weak decay rates of ${}_{\Lambda}^{12}\text{C}$ and ${}_{\Lambda}^{11}\text{B}$. The asymmetry of the weak decays and polarizations has been presented elsewhere [10].

II. EXPERIMENTAL SETUP

The present experiment was carried out at the K2 beamline [11] of the KEK 12-GeV Proton Synchrotron (PS). We constructed the spectrometer system (PIK) in order to study hypernuclei produced via (π^+, K^+) reactions in the previous experiment [12]. For the present experiment, decay counter telescopes were installed in the PIK spectrometer, as shown in Fig. 1. A platinum target of 6 mm in diameter and 60 mm in length was irradiated with typically 2.5×10^{12} protons from the KEK PS every 4 s (spill interval) with a duty factor of 50%, producing secondary pions. About 5×10^6 positive pions per spill at a momentum of 1.05 GeV/c were delivered to the experimental target through the K2 beamline. The pion beam was defined by a coincidence between beam hodoscopes BH1 and BH2. The K2 beamline provided a clean beam of pions via a static separator 6 m long operating at an electric field of 40 kV/cm. Less than a 20% positron contamination was found in the pion beam. These were rejected by anticoincidence with a gas Čerenkov counter (GC) located before BH1. A plastic scintillator was employed as an

active target (TGT). It had dimensions of 60 (wide) \times 20 (high) \times 64 (long) mm³, and was divided into two halves in height and 32 segments in length to obtain dE/dx information near to the reaction vertex [13]. Differential lucite Čerenkov counters (BLČ's) were used to discard beam pions passing through, but not interacting with, the target. Scattered particles were triggered by a scintillator hodoscope [time of flight (TOF)] located behind the PIK-PA spectrometer. Scattered kaons were triggered by a proper combination of two Čerenkov detectors, LC and AC. The LC array consisted of 11 slabs of lucite Čerenkov radiator with wavelength shifter. The AC comprised aerogel Čerenkov radiators with a refractive index of $n \sim 1.055$. The trigger condition for the (π^+, K^+) reaction was then defined by

$$\pi K = \text{BH1} \times \overline{\text{GC}} \times \text{BH2} \times \text{TGT} \times \overline{\text{BLČ}} \times \text{TOF} \times \text{LC} \times \overline{\text{AC}}.$$

Drift chambers BDC1–BDC5 and SDC1–SDC4 were tracking detectors for the incident beam pions and the scattered kaons, respectively. They were used to reconstruct particle momenta (k_{π^+} and k_{K^+}). The BDC's, SDC1, and SDC2 were drift chambers with a narrow drift space of 2.5 mm, so that they could be operated in a high-intensity beam of more than 10^6 particles per second. Drift chambers SDC3 and SDC4 were used to detect scattered particles, and were large enough to cover the solid angle of the PIK-PA spectrometer. Since the PIK-PA spectrometer had a large momentum acceptance (0.5–0.9 GeV/c), energetic protons with velocities close to that of kaons contaminated the trigger. Scattered kaons were clearly distinguished from the background par-

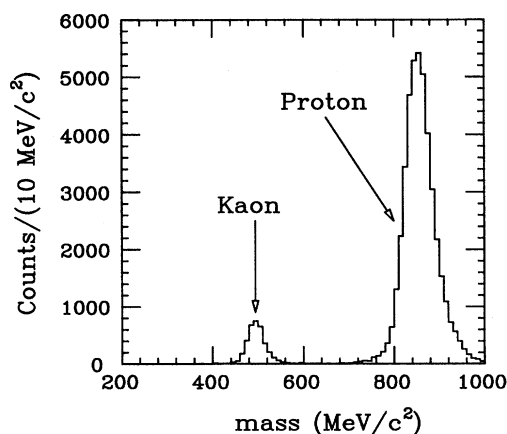


FIG. 2. Scattered particle masses reconstructed from the measured momentum and time of flight between BH2 and TOF. The kaons are clearly separated from other particles. The proton mass is slightly shifted because the velocity-reconstruction function from the time of flight is optimized for kaons.

ticles by means of mass reconstruction from the measured momentum and time of flight between BH2 and the TOF array in an off-line analysis. Figure 2 shows the mass reconstruction. The proton mass was slightly shifted because the velocity-reconstruction function from the time of flight was optimized for kaons.

Decay particles from the hypernuclei were detected by two sets of decay counter telescopes located above and below the target. Each counter telescope set comprised an array of ΔE and E counters. The E counter comprised 16 NaI detectors, each with a volume of $82 \times 82 \times 76 \text{ mm}^3$. The ΔE counter comprised four slabs of 5 mm thick plastic scintillators located in front of the E counters. Charged decay particles were identified by the ΔE counter.

Protons and negative pions from decaying hypernuclei were identified with the particle-identification (PI) function, defined by

$$F_{PI} = \alpha \ln \Delta E + b \ln E_t, \quad (3)$$

where E_t ($=\Delta E + E$ in units of MeV) is the total energy deposited in the decay counter telescopes. Coefficients a and b are ~ 0.8 and ~ 1.0 , respectively, which were determined by the Bethe-Bloch equation. Figure 3 illustrates a typical PI spectrum for decay particles of $E_t > 25 \text{ MeV}$. The pion and proton windows were set in the PI spectrum as shown in the figure. A fraction of pions contaminated the proton-gated spectrum due to impurities in the PI proton window. Similarly, the pion-gated spectrum was contaminated by the protons. The fraction of pions in the proton window to pions in the pion window was estimated to be 3.5% by extrapolating the curves, as shown in the figure. In the same manner, the fraction of protons in the pion window to protons in the proton window was found to be 6.0%. Negative pions at rest are absorbed mostly by a pn pair in a nucleus. Up to about 20% of pion annihilations release charged particles [14]. There is possibly a pion tail owing to pion annihilations, which affected the cross-contaminations of the decay par-

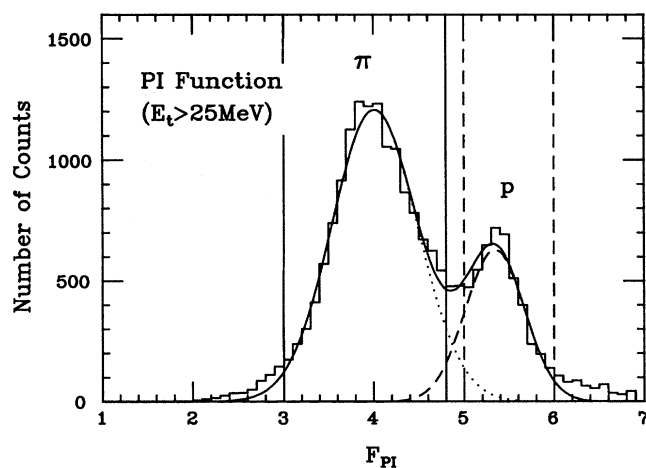


FIG. 3. Typical PI spectrum for decay particles whose energy is higher than 25 MeV. The vertical solid and dashed lines define the windows of gating pions and protons, respectively.

ticles. This was taken into account as systematic errors of the detector efficiencies mentioned in the next section.

In order to reduce the computer dead time the unbiased πK trigger was prescaled by a factor of 2. Event candidates (EVENT) were kept when they satisfied the condition

- (i) prescaled πK or
- (ii) a decay event (DECAY) in coincidence with πK .

A decay event was triggered if at least one NaI detected a particle from the target. The prescaled (π^+, K^+) events and the DECAY events were distinguished by labeling each event via a coincidence register.

Signals from the detectors were digitized by analog-to-digital converters (ADC's) and time-to-digital converters (TDC's) and were accumulated in CAMAC memory modules waiting to be read out by the data-acquisition computer. Data transfer to the computer occurred before the memory modules became filled with data. With an event size of around 600 bytes, the memory modules could accept about 30 events in the present experiment. The event rate was 60–80 per spill, and the computer trigger rate was a few per spill. The computer dead time was as small as 10%.

III. ANALYSES AND RESULTS

A. Hypernuclear excitation spectra

Figure 4 illustrates the hypernuclear excitation-energy spectra obtained using the active target. Figure 4(a) shows the (π^+, K^+) singles spectrum prescaled by a factor of 2, and Figs. 4(b) and 4(c) are the spectra in coincidence with decay protons and pions, respectively. A peak in the ground-state region can be seen at $E_x \sim 0 \text{ MeV}$. The thick target and beam counters were put in the beamline and total amount of the materials was 8.1 g/cm^2 . The energy straggling effect made the energy resolution worse by 2.3 MeV in σ . Since the resolution of the PIK spectrometer was typically 2 MeV [12], the energy resolution in the present experiment was found to be $\sigma \sim 3 \text{ MeV}$ in total. The first excited state ($E_x \sim 10 \text{ MeV}$) as well as the ground state are enhanced in the p -gated spectrum, since the NM decay probability is suppressed in the

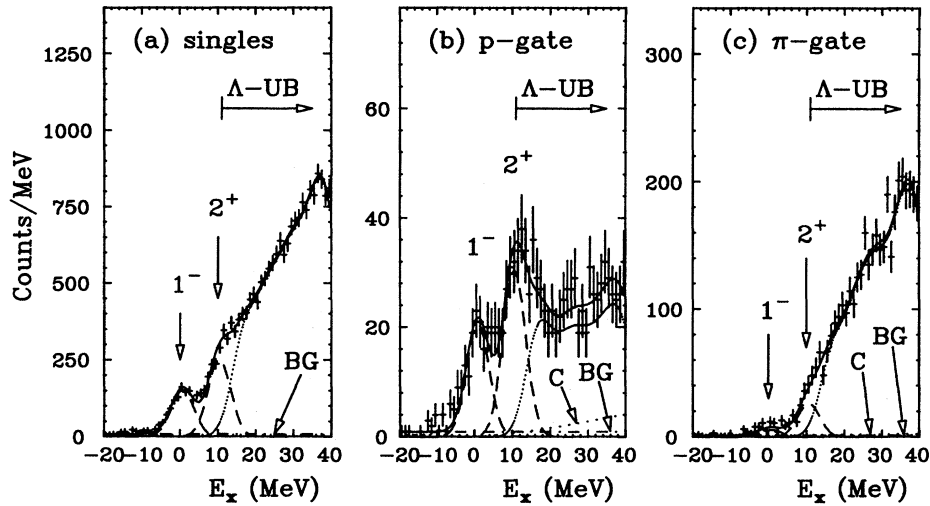


FIG. 4. (π^+, K^+) singles spectrum (a), and spectra gated by the decay protons (b) and by the decay pions (c). The curves indicate the structure of the spectra obtained by the fitting procedure FIT-1. In FIT-1, two Gaussian peaks of $\sigma \sim 3$ MeV at $E_x = 0$ MeV (1^-) and $E_x = 10$ MeV (2^+) and the calculated states from Ref. [18] in the Λ -unbound (Λ -UB) region ($E_x > 11$ MeV) were assumed. Contamination (C) of pions in the proton-gated spectrum because of the impurity in the PI window for protons was corrected. A corresponding correction was made to the pion-gated spectra. The background (BG) estimated from that in the $E_x < -10$ MeV region was subtracted from each spectrum.

Λ -unbound region ($E_x > 11$ MeV), and are sufficiently clear to obtain a yield for each peak.

The ground and first excited states correspond to the n -hole Λ -particle states of $[p^{-1}s_\Lambda]$ and $[p^{-1}p_\Lambda]$, respectively. A calculation [15] indicates that the (π^+, K^+) reaction mainly populates the 1^- and 2^+ states in the ground and the first excited states of ${}_{\Lambda}^{12}\text{C}$, respectively. The 2^+ state is unstable against a proton emission and forms ${}_{\Lambda}^{11}\text{B}$. These states have been well established through studies of hypernuclear production at CERN, BNL, and KEK [12,16,17]. We thus assumed in the fitting procedure to extract the peak yields that two Gaussian peaks with $\sigma \sim 3$ MeV are located at $E_x = 0$ and 10 MeV.

The region above $E_x \sim 11$ MeV is open for the Λ -escape channel (Λ -unbound region). To reproduce the spectrum shape of this continuum region we used the calculated states from Ref. [18]. Each state was folded with a Gaussian resolution function of $\sigma \sim 3$ MeV in the present fitting procedure (FIT-1). Even in this region, a certain fraction of the states may form a hyperfragment through the Λ -spreading process [19]. These are characterized by the compound process where the intermediate state populated by the reaction decays into a daughter nucleus statistically. Since the hyperfragments can emit protons through NM decays the same fitting procedure could be used for the p -gated spectrum.

In a separate fitting procedure we assumed that the spectrum shape in the Λ -unbound region could be represented by a function as follows:

$$f(x) = \frac{1}{\sqrt{\pi}\sigma} \int g(x - x_{\text{th}} + q) \exp\left(-\frac{q^2}{2\sigma^2}\right) dq, \quad (4)$$

$$g(t) = \begin{cases} a\sqrt{t} + b + ct + dt^2 + et^3 + ft^4 & \text{for } t > 0 \\ 0 & \text{otherwise,} \end{cases} \quad (5)$$

where x_{th} is the threshold energy for quasifree Λ production. The threshold behavior and the gross features of the quasifree spectrum were represented by square-root and polynomial functions. They were smeared by a Gaussian resolution function of $\sigma \sim 3$ MeV (FIT-2).

All of the spectra applied to the fitting procedure were corrected in the following ways.

(a) The fraction estimated to be due to pion decays was subtracted from the proton-gated spectrum. A corresponding correction was made to the pion-gated spectrum.

(b) The background in each spectrum was estimated from that in the region $E_x < -10$ MeV, where no (π^+, K^+) process should take place. We assumed that the background was flat (constant) over the spectra, since the number of spurious (π^+, K^+) events seen in the spectra is quite low.

The curves in Figs. 4 and 5 demonstrate the structure of the spectra in the cases of FIT-1 and FIT-2, respectively. Both cases reproduced similar spectra. We took the averages of the peak yields obtained in the two cases. The differences were included in the systematic errors.

B. Energy spectrum of NM decay protons

The energy spectrum of NM decay nucleons is affected by several nuclear effects. To estimate the energy distribution of the nucleons ejected from the hypernuclei, the effects of the Fermi motion and intranuclear cascade were studied using a Monte Carlo simulation. The simulation included three major parts: (i) *the initial NM decay*, (ii) *the intranuclear cascade*, and (iii) *the evaporation process*. Details concerning the simulation are described in the Appendix.

(i) *The initial NM decay*. We considered the transition $\Lambda N \rightarrow NN$ in the initial NM decay. The momentum distributions of the initial ΛN in the hypernucleus determine those of the final NN . The initial momentum distributions were

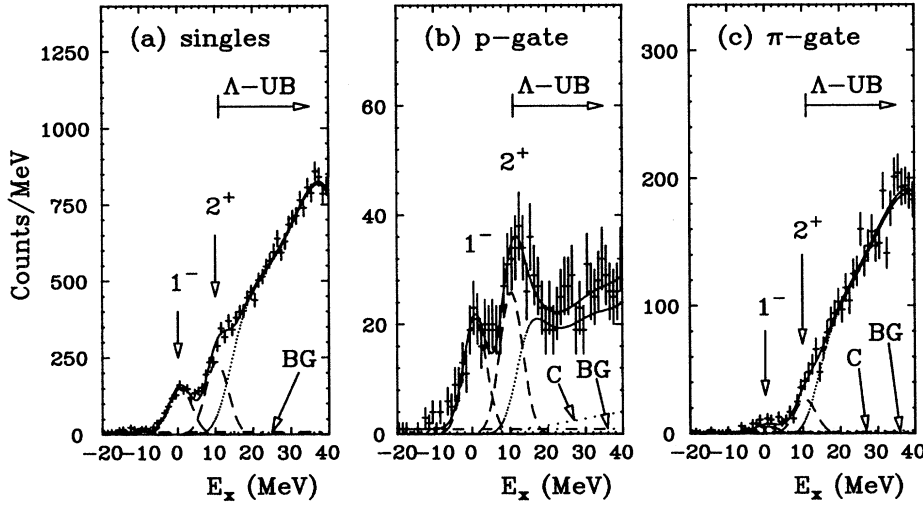


FIG. 5. Same as Fig. 4, but the fitting procedure FIT-2 was used to reproduce the spectra.

given by the wave functions of Λ and N , respectively. A point interaction in the $\Lambda N \rightarrow NN$ process was assumed.

(ii) *The intranuclear cascade.* The intranuclear cascade process was described by scatterings of the decay nucleons with nucleons in the residual nucleus. The interaction cross sections were determined by the mean free path obtained from the imaginary part of the optical potential. We considered only s -wave scatterings. The scattered nucleons were trapped by the residual nucleus when they were below the Fermi surface and the nucleus was excited.

(iii) *The evaporation process.* Nucleon evaporations from the excited residual nucleus took place after the intranuclear cascade. The spectrum was assumed to be characterized by an exponential function of the nuclear temperature.

Figure 6(a) shows a simulated energy spectrum of protons from the $\Lambda p \rightarrow pn$ process in ^{12}C . One can see that the spectrum is characterized by three major components. Protons from the evaporation process are characterized by the exponential shape in the low-energy region. Bumps with a peak at around 60 MeV and a peak at around 80 MeV correspond to

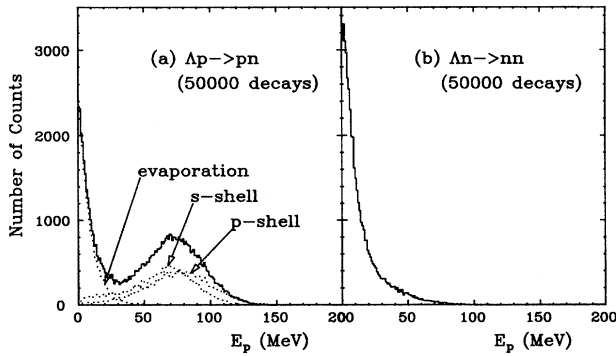


FIG. 6. Proton-energy (E_p) spectrum from the $\Lambda p \rightarrow pn$ process in ^{12}C obtained by a Monte Carlo simulation (a). Three major components (protons from the evaporation process, those from the s shell, and those from the p shell) are shown. The simulated proton-energy spectrum from the $\Lambda n \rightarrow nn$ process in ^{12}C is shown in (b).

protons from the s shell and the p shell, respectively. The probability of a second process, such as evaporation and collisions, is estimated to be about 20%. Figure 6(b) shows the energy distribution of protons related to the $\Lambda n \rightarrow nn$ process. The cutoff for the low-energy protons makes the contribution from the second process small.

It is also necessary to estimate the geometrical effects as follows. Since the present experiment had no tracking detector for the decay particles, the vertex point could not be determined precisely enough to make corrections for energy losses of the decay particles in the target material. Particles passing through the edge of the decay counter volume also distort the energy spectrum. We employed a Monte Carlo calculation to determine the detector response and to estimate the detection efficiency for the decay particles, including the solid angle and the PI function efficiency.

Figure 7 shows the proton-energy spectrum detected by the decay counter in the simulation for the $\Lambda p \rightarrow pn$ process (histogram) together with that measured for the ground-state region (plotted with closed circles). The measured E_p spectrum was corrected for pion contamination. The simulation reproduced the present experimental data quite well.

Here, although we approximated the transition $\Lambda N \rightarrow NN$ with a point interaction, it may depend upon the ΛN spin configuration. As can be seen in Fig. 6(a), the s -shell and p -shell nucleons gave different spectra. Changes in the ratio of the s -shell component to the p -shell component affect the estimation of the solid angles. We considered two extreme cases. One is the case in which only the s -shell component contributes to the spectrum. The other is the case using only the p -shell component. The difference was taken into account as systematic errors on the solid angles.

We obtained the solid angles $\varepsilon_p \Omega_p = 24.5^{+1.6}_{-8.1}\%$ and $\varepsilon_n \Omega_p = 0.8^{+1.0}_{-0.7}\%$ for ^{12}C , and $\varepsilon_p \Omega_p = 23.5^{+1.3}_{-6.4}\%$ and $\varepsilon_n \Omega_p = 0.8^{+1.0}_{-0.4}\%$ for ^{11}B , respectively, where the ε_p and the ε_n represent the efficiency for detected protons with $E_p > 45$ MeV in the $\Lambda p \rightarrow pn$ and $\Lambda n \rightarrow nn$ processes. The errors include also the systematic errors due to pion annihilations.

C. Branching ratios and weak decay partial rates

By definition, the branching ratios $R = \Gamma_n / \Gamma_p$, $b_p = \Gamma_p / \Gamma_{\text{tot}}$, and $b_{nm} = \Gamma_{nm} / \Gamma_{\text{tot}}$ satisfy the relationship

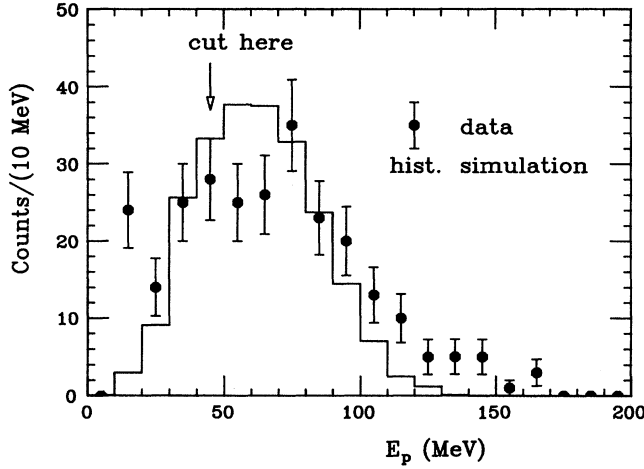


FIG. 7. Proton-energy (E_p) spectrum observed in the ground-state region (circles with error bars). The histogram was obtained by a simulation in which the geometry of the decay counter telescopes and the energy loss effect in the materials were considered. The energy distribution of the protons obtained by the intranuclear cascade calculation was used as an input of the simulation.

$$b_{nm} = (1 + R) \times b_p. \quad (6)$$

Here, Γ_{tot} represents the total decay rate of a Λ hypernucleus. The quantities b_p and b_{nm} are the branching ratios of the $\Lambda p \rightarrow pn$ process and the total NM decay, respectively. The observed protons also include those which originate in the $\Lambda n \rightarrow nn$ process, since a proton may be kicked out of the nucleus in the intranuclear cascade process. Protons may also be observed when the M decay pions are absorbed in the residual nuclei. In practice, we cannot distinguish the pion-absorbed M decay from the NM decays. It is, however, interesting to examine the fraction of NM decay events which are caused by real pion absorption. Assuming that the pion-absorbed M decays yielded a proton-energy spectrum close to that of the NM decays, we obtained

$$b_p = \frac{Y_p}{Y_s} [(R\varepsilon_n + \varepsilon_p)\Omega_p]^{-1}, \quad (7)$$

where Y_s and Y_p denote the peak yields observed in the singles and proton-gated hypernuclear excitation-energy spectra, respectively. The quantity b_{nm} can be written as a branching ratio of the mesonic process ($\Gamma_m/\Gamma_{\text{tot}}$) as follows:

TABLE I. Branching ratios for mesonic π^- decay (b_{π^-}). The first and second errors appearing in the results stand for the statistical and systematic errors, respectively. Other experimental results concerning mesonic π^0 decay (b_{π^0}) and theoretical calculations concerning the ratios (r_π) of π^0 decay to π^- decay are listed for reference.

	Experiment		Theory [22]		
	b_{π^-} Present	b_{π^0} Sakaguchi <i>et al.</i> [20]	Free	r_π MSU	WHIS
${}_{\Lambda}^{12}\text{C}$	$0.11 \pm 0.05 \pm 0.02$	$0.174 \pm 0.057 \pm 0.008$	1.35	1.26	1.18
${}_{\Lambda}^{11}\text{B}$	$0.17 \pm 0.04 \pm 0.02$	$0.140 \pm 0.039 \pm 0.025$	0.47	0.48	0.47

TABLE II. Branching ratios for NM proton decay (b_p), total NM decay (b_{nm}), and ratios (R) of NM neutron decay to NM proton decay. The first and second errors appearing in all of the entries indicate the statistical and systematic errors, respectively.

${}_{\Lambda}^AZ$	b_p	b_{nm}	R
${}_{\Lambda}^{12}\text{C}$	$0.25 \pm 0.04^{+0.09}_{-0.03}$	$0.71 \pm 0.07 \pm 0.02$	$1.87 \pm 0.59^{+0.32}_{-1.00}$
${}_{\Lambda}^{11}\text{B}$	$0.22 \pm 0.04^{+0.06}_{-0.03}$	$0.69 \pm 0.05 \pm 0.03$	$2.16 \pm 0.58^{+0.45}_{-0.95}$

$$b_{nm} = 1 - \frac{\Gamma_m}{\Gamma_{\text{tot}}} = 1 - (1 + r_\pi) \frac{Y_{\pi^-}}{Y_s} [\varepsilon_{\pi^-} \Omega_{\pi^-}]^{-1}, \quad (8)$$

where r_π is the ratio of π^0 decays to π^- decays (b_{π^0}/b_{π^-}). The quantity Y_{π^-} denotes the peak yield observed in the pion-gated hypernuclear excitation-energy spectrum. We estimated the detection efficiency and the solid angle for negative pions ($\varepsilon_{\pi^-} \Omega_{\pi^-}$) using a Monte Carlo simulation; the results were $\varepsilon_{\pi^-} \Omega_{\pi^-} = 0.19 \pm 0.02$ and $\varepsilon_{\pi^-} \Omega_{\pi^-} = 0.31 \pm 0.03$ for ${}_{\Lambda}^{12}\text{C}$ and ${}_{\Lambda}^{11}\text{B}$, respectively. They were obtained for pions with $E_t > 25$ MeV. The errors were due to a possible pion tail in the PI spectrum and contributed to the systematic errors.

We obtained $b_{\pi^-} = 0.11 \pm 0.05 \pm 0.02$ for ${}_{\Lambda}^{12}\text{C}$ and $0.17 \pm 0.04 \pm 0.02$ for ${}_{\Lambda}^{11}\text{B}$, as shown in Table I. The first and second errors stand for the statistical and systematic errors, respectively. We made use of data from previous studies of the π^0 -mesonic decay rate in order to evaluate the quantities b_{nm} , b_p , and R . The experimental measurements of the π^0 decay branching ratio (b_{π^0}) [20] are listed in Table I. We thus obtained the quantities b_p , b_{nm} , and R from Eqs. (6)–(8), as shown in Table II.

The total decay rates were measured as 1.25 ± 0.18 for ${}_{\Lambda}^{12}\text{C}$ and 1.37 ± 0.16 for ${}_{\Lambda}^{11}\text{B}$ in units of the decay rate of the Λ hyperon in free space (Γ_Λ) by Grace *et al.* [7]. From these values and the obtained branching ratios, we derived the decay partial rates (Γ_{π^-} , Γ_p , and Γ_{nm}), as listed in Tables III and IV.

IV. DISCUSSIONS

A. M decay rates

The present results for Γ_{π^-} are summarized in Table III, and are compared with results from other relevant studies. The BNL experiment reported $\Gamma_{\pi^-} = (0.052^{+0.063}_{-0.035})\Gamma_\Lambda$ in ${}_{\Lambda}^{12}\text{C}$ [8]. This value does not contradict the present results concerning Γ_{π^-} in ${}_{\Lambda}^{12}\text{C}$. In the BNL experiment a large number of background events remained in the hypernuclear

TABLE III. Present results for Γ_{π^-} . The previous measurements and calculations are listed for a comparison. All of the entries are in units of the free Λ decay width (Γ_Λ), but for ratios of Γ_{π^-} in ${}^{12}\text{C}$ to that in ${}^{11}\text{B}$.

	Present	Experiment		Theory [22]		
		BNL [8]	Montwill <i>et al.</i> [21]	Free	WHIS	MSU
$\Gamma_{\pi^-}({}^{12}\text{C})/\Gamma_\Lambda$	$0.14 \pm 0.07 \pm 0.03$	$0.052^{+0.063}_{-0.035}$		0.058	0.107	0.134
$\Gamma_{\pi^-}({}^{11}\text{B})/\Gamma_\Lambda$	$0.23 \pm 0.06 \pm 0.03$		0.22 ± 0.05	0.134	0.223	0.294
$\Gamma_{\pi^-}({}^{12}\text{C})/\Gamma_{\pi^-}({}^{11}\text{B})$	$0.61 \pm 0.31 \pm 0.15$			0.433	0.480	0.456

excitation-energy spectrum in the inclusive (K^- , π^-) reactions on ${}^{12}\text{C}$. This possibly makes Γ_{π^-} small. They also reported an upper limit of $0.16\Gamma_\Lambda$ at the 95% confidence level. The present (π^+ , K^+) experiment has kept the number of background events small in the excitation-energy spectrum. Montwill *et al.* have reported $Q^- = \Gamma_{nm}/\Gamma_{\pi^-} = 4.8 \pm 1.1$ in ${}^{11}\text{B}$ [21]. Here, we can extract a value for Γ_{π^-} of $(0.22 \pm 0.05)\Gamma_\Lambda$ from the following equations:

$$\Gamma_{\pi^0}/\Gamma_{\pi^-} = 0.5, \quad (9)$$

$$\Gamma_{\text{tot}} = \Gamma_{nm} + \Gamma_{\pi^-} + \Gamma_{\pi^0}, \quad (10)$$

as assumed in Ref. [20]. Equation (9) is required due to the empirical $\Delta I = 1/2$ rule. The assumption is reasonable since no significant difference of the shell structure between the daughter nuclei in the π^- and π^0 decays of ${}^{11}\text{B}$ affects the ratio. We can also extract a value for Γ_{π^-} of $(0.21 \pm 0.04)\Gamma_\Lambda$ using the ratio $\Gamma_{\pi^0}/\Gamma_{\pi^-} = r_\pi$ obtained from the present b_{π^-} and the previous b_{π^0} [20]. The present measurement of Γ_{π^-} in ${}^{11}\text{B}$ agrees well with both extracted values.

It has been suggested that the suppression of M decay is weakened, even in heavy hypernuclei, because the pion wave distortion and nucleon correlation in the nuclear medium make the decay probability large [1,2]. Motoba, Itonaga, and Bandō have studied the effects of pion distortion on p -shell hypernuclei by employing three different potentials, as shown in Table III [22]. ‘‘Free’’ means no distortion. The MSU potential gave a larger distortion, and thus a larger Γ_π than that given by another potential indicated as WHIS. The

present result concerning Γ_{π^-} in ${}^{12}\text{C}$ is close to that given by WHIS, although it does not contradict the others within errors. Γ_{π^-} in ${}^{11}\text{B}$ is sensitive to the potential. The present Γ_{π^-} in ${}^{11}\text{B}$ agrees well with that given by WHIS. The ratio of Γ_{π^-} in ${}^{12}\text{C}$ to that in ${}^{11}\text{B}$ is found to be $0.61 \pm 0.34 \pm 0.15$ in the present experiment. This value agrees with the calculations which are almost independent of the potentials. The present results show the effect of pion wave distortion on the M decay rate.

B. NM decay rates

The obtained $\Gamma_{nm}/\Gamma_\Lambda$ and Γ_n/Γ_p are displayed in Table IV together with previous measurements and theoretical calculations. We can extract $\Gamma_{nm} = (1.06 \pm 0.34)\Gamma_\Lambda$ in ${}^{11}\text{B}$ from the Q^- given by Montwill *et al.* [21] employing Eqs. (9) and (10). The present results concerning Γ_{nm} show almost unity in units of Γ_Λ , and agree well with the previous measurements. The BNL experiment measured neutrons and protons stimulated from the hypernuclei [8]. The large errors are due to low efficiencies and large backgrounds in neutron detection. The present experiment found that Γ_n is almost twice the size of Γ_p in both ${}^{12}\text{C}$ and ${}^{11}\text{B}$, although the results have sizable errors. Mangotra *et al.* [23] and Montwill *et al.* [21] reported $\Gamma_n/\Gamma_p = 2.11^{+0.36}_{-0.29}$ and $0.59^{+0.17}_{-0.14}$, respectively. Both emulsion experiments failed to identify the hypernuclear isotope.

Dubach has reported the NM decay rates in nuclear matter based on meson-exchange models, and assumed a relative s wave in the initial ΛN system [4]. Their one-pion exchange

TABLE IV. Present results for Γ_p , Γ_{nm} , and Γ_n/Γ_p . The previous measurements and calculations in p -shell hypernuclei are listed for reference. All of the entries are in units of the free Λ decay width (Γ_Λ), but for Γ_n/Γ_p 's.

${}^A_\Lambda Z$	Γ_p/Γ_Λ	$\Gamma_{nm}/\Gamma_\Lambda$	Γ_n/Γ_p	Refs.
Experiment				
${}^{12}_\Lambda\text{C}$	$0.31 \pm 0.07^{+0.11}_{-0.04}$	$0.89 \pm 0.15 \pm 0.03$	$1.87 \pm 0.59^{+0.32}_{-1.00}$	present
${}^{11}_\Lambda\text{B}$	$0.30 \pm 0.07^{+0.08}_{-0.04}$	$0.95 \pm 0.13 \pm 0.04$	$2.16 \pm 0.58^{+0.45}_{-0.95}$	present
$A > 10$			$2.11^{+0.36}_{-0.29}$	[23]
${}_\Lambda\text{B}, {}_\Lambda\text{C}, {}_\Lambda\text{N}$			$0.59^{+0.17}_{-0.14}$	[21]
${}^{12}_\Lambda\text{C}$		1.14 ± 0.20	$1.33^{+1.12}_{-0.81}$	[8]
${}^{11}_\Lambda\text{B}$			$1.04^{+0.59}_{-0.48}$	[8]
Theory				
$A = \infty$		1.23	0.34	[4]
${}^{12}_\Lambda\text{C}$		1.28		[24]
${}^{12}_\Lambda\text{C}$		0.98	0.27	[5]

calculation gave a large Γ_{nm} of 2–4 and a very small Γ_n , where the tensor term was strongly enhanced and the neutron-induced transition was forbidden. It is reasonable to take the short-range effects into account since the $\Lambda N \rightarrow NN$ transition involves a large momentum transfer of ~ 400 MeV/c. Dubach also reported heavier meson effects in the calculation. Considering π , ρ , η , ω , K , and K^* , they obtained $\Gamma_{nm} = 1.23\Gamma_{\Lambda}$ and $\Gamma_n/\Gamma_p = 0.34$, which improved the calculated values, but still suppressed Γ_n . Cheung, Heddle, and Kisslinger calculated Γ_{nm} by employing the quark hybrid model, where the six-quark state was taken into account in the short-range region. They obtained $\Gamma_{nm} = 1.28\Gamma_{\Lambda}$ in ${}_{\Lambda}^{12}\text{C}$ using the $\Delta I = 1/2$ rule [24]. The value is consistent with the measured Γ_{nm} . Ramos *et al.* calculated the NM decay rates in finite hypernuclei, ${}_{\Lambda}^5\text{He}$, ${}_{\Lambda}^{11}\text{B}$, and ${}_{\Lambda}^{12}\text{C}$, based on a one-pion exchange model with a relativistic nuclear treatment [25]. The authors have pointed out that the contribution of a p -shell nucleon is of importance to the decay amplitudes. The calculation gave the parity-violating and parity-conserving amplitudes, and reproduced the asymmetry of protons in the NM decay from polarized hypernuclei. This has been reported elsewhere [10]. They have reported $\Gamma_{nm} = 0.87\Gamma_{\Lambda}$ and $\Gamma_n/\Gamma_p = 0.30$ for π , ρ , η , ω , K , and K^* meson exchanges in ${}_{\Lambda}^{12}\text{C}$ [5]. Although the Γ_{nm} is in good agreement with the measured values, the Γ_n/Γ_p is still quite different from the measured values.

Ericson *et al.* have suggested that multinucleon-induced processes, such as $\Lambda NN \rightarrow NNN$, play an important role in NM decay [6]. The process is caused by the absorption of a virtual (off-shell) pion from a decaying Λ into a pair of nucleons or more. It reflects the propagation of the pion through the nuclear medium, which is strongly related to the M decay process. Recently Ramos, Oset, and Salcedo made more realistic calculations and reported $\Gamma^{(2)} = 1.45$ and $\Gamma^{(3)} = 0.27$ (in units of Γ_{Λ}) for ${}_{\Lambda}^{12}\text{C}$, where superscript (2) and (3) mean two-body and three-body NM decays, respectively. The measured NM decay rates are expected to be decomposed into $\Gamma^{(2)}$ and $\Gamma^{(3)}$. The present Γ_{nm} were obtained from $\Gamma_{\text{tot}} - \Gamma_m$, and we write $\Gamma_{nm} = \Gamma_p^{(2)} + \Gamma_n^{(2)} + \Gamma^{(3)}$. As was also mentioned in Ref. [26], we assume the $\Lambda pn \rightarrow pnn$ channel is dominant in three-body decay. Then, the measured Γ_p and Γ_n can be expressed as

$$\Gamma_p = \Gamma_p^{(2)} + f\Gamma^{(3)}, \quad (11)$$

$$\Gamma_n = \Gamma_n^{(2)} + (1-f)\Gamma^{(3)}. \quad (12)$$

Here, f is the factor in order to correct for the difference of the efficiency for two-body-decay protons from that for three-body-decay protons because of a discrimination for low-energy protons. Multinucleon-induced decay would feed the low-energy region in the proton-energy spectrum because the released energy is shared by three particles or more. One expects f less than 1. Equations (11) and (12) lead to

$$\frac{\Gamma_n^{(2)}}{\Gamma_p^{(2)}} = \frac{\Gamma_n}{\Gamma_p} \frac{1 - (\Gamma_p/\Gamma_n + 1)(1-f)[\Gamma^{(3)}/\Gamma_{nm}]}{1 - (\Gamma_n/\Gamma_p + 1)f[\Gamma^{(3)}/\Gamma_{nm}]}. \quad (13)$$

The correction of multinucleon-induced process depends upon f . The measured Γ_n/Γ_p is corrected to be small when the factor f is less than Γ_p/Γ_{nm} . Deconvolution of the

proton-energy spectrum is required to obtain f , and then the corrected $\Gamma_n^{(2)}/\Gamma_p^{(2)}$ can be compared with the theoretical calculations. It is necessary to know the energy-differential three-body decay rate and to take into account the change of the nucleon-energy spectrum due to the nuclear effects.

The structure of the nucleon-energy spectrum may be sensitive to the detailed mechanism involved in hypernuclear NM decays. In particular, the structure of the low-energy region is useful for studying the multinucleon process. A precise measurement of low-energy protons, and also neutrons if possible, from the NM decay is required to study the problem further.

V. CONCLUSIONS

In the present study we measured the M decay and NM decay rates, which are key observables for studying weak decays. The measured Γ_{π^-} shows that Pauli blocking is less effective due to pion distortion than expected in ${}_{\Lambda}^{12}\text{C}$ and ${}_{\Lambda}^{11}\text{B}$. The previous Γ_{π^0} measurement in ${}_{\Lambda}^{12}\text{C}$ and ${}_{\Lambda}^{11}\text{B}$ also suggested a strong distortion effect, although it was much stronger than that predicted by a calculation [20,22]. Both experiments demonstrate that pion distortion in the nuclear medium plays an important role in the suppression of hypernuclear mesonic decay. Systematic measurements with a mass number dependence are necessary for a further understanding of M decays.

The present result concerning Γ_{nm} is consistent with previous measurements and in good agreement with the theoretical calculations. The present measurement shows that Γ_n is almost twice the size of Γ_p , although the obtained Γ_n/Γ_p ratios in ${}_{\Lambda}^{12}\text{C}$ and ${}_{\Lambda}^{11}\text{B}$ have sizable errors. The previous measurements gave a ratio of almost unity, while the calculations suggested a more strongly suppressed Γ_n . There are still discrepancies between the experimental values and the theoretical calculations. The multinucleon-induced process in NM decay may account for this discrepancy. Precise studies on the structure of the nucleon-energy spectrum, particularly in the low-energy region, are needed to examine the multinucleon process in NM decays.

ACKNOWLEDGMENTS

The authors thank Professor H. Sugawara, Professor K. Nakai, Professor K. Takamatsu, Professor M. Takasaki, Professor T. Sato, Professor J. Chiba, Professor T. K. Ohoka, Professor M. Kihara, and the crew of the KEK PS for their support and encouragement to carry out the experiment. They are grateful to the collaborators of the present E160 experiment.

APPENDIX

1. Monte Carlo simulation

We considered a phenomenological model for the NM decay process to estimate the energy distribution of the stimulated nucleons. The process includes three major parts: (i) *the initial NM decay*, (ii) *the intranuclear cascade*, and (iii) *the evaporation process*, as mentioned in Sec. III B.

We can describe the momentum distribution of the two nucleons in the final channel of the NM decay as follows:

TABLE V. Woods-Saxon potential parameters used for calculating the wave functions. BE denotes the binding energy of Λ and N . The quantities a and c represent the diffusivity and radius of the potential, respectively. V_0 and V_{so} are the potential depth corresponding to the leading and spin-orbit forces, respectively.

		BE ($s_{1/2}$) (MeV)	BE ($p_{3/2}$) (MeV)	a (fm)	c (fm)	V_0 (MeV)	V_{so} (MeV)
$^{12}_\Lambda\text{C}$	Λ	10.8		0.54	2.79	25.5	
^{11}C	p	24.8	8.69	0.54	2.52	54.8	5.0
	n	30.3	13.1	0.54	2.52	57.2	5.0
$^{11}_\Lambda\text{B}$	Λ	10.2		0.54	2.72	25.3	
^{10}B	p	21.5	6.59	0.54	2.49	46.1	5.0
	n	24.1	8.44	0.54	2.49	49.7	5.0

$$\frac{d^6 D(\mathbf{p}_1, \mathbf{p}_2)}{d\mathbf{p}_1 d\mathbf{p}_2} = |\langle N_1 \mathbf{p}_1 N_2 \mathbf{p}_2; A-2 | V_{\Lambda N} | \Lambda Z \rangle|^2, \quad (\text{A1})$$

where $| \Lambda Z \rangle$ represents the initial hypernuclear state; the final state is expressed by the two-nucleon state of N_1 and N_2 with momenta of \mathbf{p}_1 and \mathbf{p}_2 and the residual nuclear state of mass number $A-2$. The quantity $V_{\Lambda N}$ stands for the potential driving the $\Lambda N \rightarrow NN$ transition. The $V_{\Lambda N}$ interaction is characterized by short-range effects, since the $\Lambda N \rightarrow NN$ transition involves a large momentum transfer of ~ 400 MeV/c. We approximated $V_{\Lambda N}$ by a point interaction. We considered the plane waves of the final two nucleons and solved Eq. (A1) as

$$\frac{d^6 D(\mathbf{p}_1, \mathbf{p}_2)}{d\mathbf{p}_1 d\mathbf{p}_2} = \sum_{\alpha} \int d\mathbf{k}_{\Lambda} |\phi^{\Lambda}(\mathbf{k}_{\Lambda})|^2 \int d\mathbf{k}_N |\phi_{\alpha}^N(\mathbf{k}_N)|^2 \delta(p_1 + p_2 - p_{\Lambda} - p_N). \quad (\text{A2})$$

Here, we required both energy and momentum conservation in the $\Lambda N \rightarrow NN$ transition. $p_{\Lambda} = (E_{\Lambda}, \mathbf{k}_{\Lambda})$, $p_N = (E_N, \mathbf{k}_N)$, $p_1 = (E_1, \mathbf{p}_1)$, and $p_2 = (E_2, \mathbf{p}_2)$ denote the four-momenta of the initial Λ and N and the final two nucleons, respectively. Since the initial Λ is bound, the total energy (E_{Λ}) is described as

$$E_{\Lambda} = m_{\Lambda} - B_{\Lambda} - \frac{|\mathbf{k}_{\Lambda}|^2}{2M_R}, \quad (\text{A3})$$

where B_{Λ} stands for the Λ -separation (Λ -binding) energy; m_{Λ} and M_R are the masses of the Λ and the residual nucleus. The momentum distributions of the Λ and N were given by the momentum-space wave functions, $\phi^{\Lambda}(\mathbf{k}_{\Lambda})$ and $\phi_{\alpha}^N(\mathbf{k}_N)$, in the initial state. The subscript α represents the shell (orbital) of the nucleon. We assumed that Λ lies in the s orbital before the NM decay.

The decay nucleons may be scattered by the nucleons in the residual nucleus. The scattering probability depends upon the Λ and N densities and the mean free path $[\lambda(\mathbf{p})]$. Here, we write the density distribution of the ΛN and the thickness of the nucleus measured in units of the mean free path in Eqs. (A4) and (A5), respectively:

$$\rho_{\alpha}^{\Lambda N}(\mathbf{r}) = \int d(\mathbf{r}') |\psi^{\Lambda}(\mathbf{r}) \psi_{\alpha}^N(\mathbf{r}')|^2 \delta(\mathbf{r} - \mathbf{r}'), \quad (\text{A4})$$

$$\tilde{T}(\mathbf{r}, \mathbf{e}; \mathbf{p}) = \int \frac{dz}{\lambda(\mathbf{p})} \frac{\rho_N(\mathbf{r} + z\mathbf{e})}{\rho_N(0)}, \quad (\text{A5})$$

where ψ^{Λ} and ψ_{α}^N are the coordinate representations of the Λ and N wave functions. \tilde{T} is the thickness seen from position \mathbf{r} in the direction \mathbf{e} , and ρ_N represents the nucleon-density distribution of the residual nucleus.

In practice, it is complicated to unify the initial NM decay with the intranuclear cascade process. A method to do this can be found in a study by Chiang and Hüfner [14]. We employed a Monte Carlo simulation. In the simulation the initial NM decay took place according to Eq. (A2). The decay nucleons were then allowed to scatter until they were emitted or trapped by the nucleus. A NM decay point was given by Eq. (A4) and the scattering point was evaluated from Eq. (A5). We calculated single particle wave functions for the ϕ 's and ψ 's, as described in the next subsection. The mean free path was estimated from the imaginary part of the optical potential [27]. We then considered s -wave scatterings in the initial NM decay and the intranuclear cascade. The scattered nucleons cannot escape from the nucleus when their total energies in the two-body center-of-mass frame are below the nucleon mass (they would be below the Fermi surface). They are consequently trapped by the nucleus and excited the nucleus.

Nucleon evaporations from the excited residual nucleus took place after the intranuclear cascade. The spectrum was assumed to be characterized by an exponential function of the nuclear temperature.

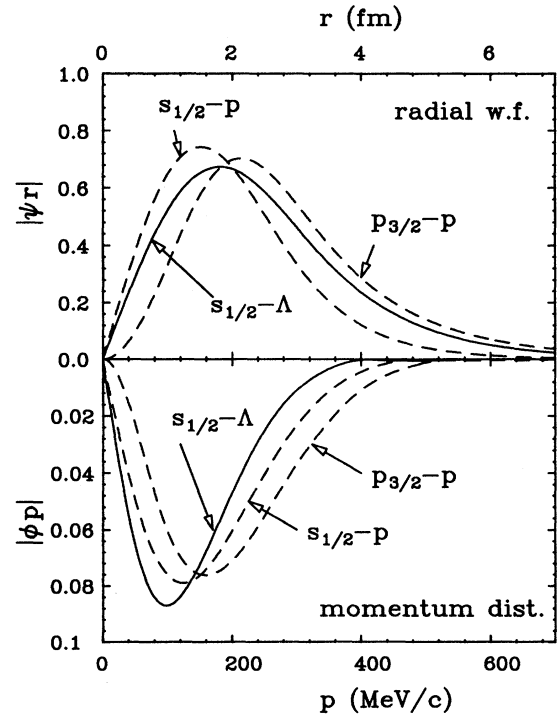


FIG. 8. Density distributions of the radial wave functions obtained for the s -shell hyperon, the s -shell proton, and the p -shell proton in ^{12}C (upper). The momentum distributions of the Λ and N were given by the momentum-space wave functions (lower).

When a Λ hyperon is polarized by the (π^+, K^+) reaction at a finite scattering angle, NM decay protons have an asymmetric angular distribution of $W(\theta) \sim 1 + P_{\Lambda} A_1 \cos\theta$, where P_{Λ} and A_1 represent the Λ -spin polarization and the asymmetry parameter, respectively [28,29]. The second term introduces a so-called up-down asymmetry with respect to the reaction plane defined by $\mathbf{k}_{\pi^+} \times \mathbf{k}_{K^+}$. A measurement of the asymmetry for the NM decay protons is another interesting subject, and a goal of the PS E160 experiment. This has already been reported elsewhere [10]. The nuclear effects modify the angular distribution and attenuate the asymmetry. We also evaluated the attenuation factor by means of the simulation code.

2. Wave functions

We used the Woods-Saxon potential to obtain single particle wave functions of the hyperon and nucleons. It is described as

$$V(r) = V_0 f(r) + V_{\text{so}} \left(\frac{\hbar}{m_{\pi} c} \right)^2 \frac{1}{r} \frac{df}{dr} (\mathbf{l} \cdot \boldsymbol{\sigma}) + V_C, \quad (\text{A6})$$

where

$$f(r) = \left[1 + \exp \left(\frac{r-c}{a} \right) \right]^{-1}. \quad (\text{A7})$$

Here, V_C represents the Coulomb potential assuming a uniform charge distribution inside the nuclear radius (c). Parameters relevant to the potential are summarized in Table V. The V_0 's were adjusted so as to reproduce the given separation energy, for which the binding energy in the $p_{3/2}$ nucleon [30] and $s_{1/2}$ Λ [31] were used. The V_{so} 's were assumed to be 5 MeV for the nucleons, and negligible for the hyperon [32–34]. The binding energies of $s_{1/2}$ nucleons were obtained by the given potential. Figure 8 displays the radial wave functions obtained for the s -shell hyperon (solid line), the s -shell proton (dashed line), and the p -shell proton (dotted line) in ${}^{\Lambda}_{12}\text{C}$. The momentum distributions of the hyperon and nucleons in the hypernuclei are also displayed in the same figure.

-
- [1] H. Bandō and H. Takaki, *Prog. Theor. Phys.* **72**, 106 (1984); *Phys. Lett.* **150B**, 409 (1985); H. Bandō, *Prog. Theor. Phys. Suppl.* **81**, 181 (1985).
- [2] E. Oset and L. L. Salcedo, *Nucl. Phys.* **A443**, 704 (1985).
- [3] K. Takeuchi, H. Takaki, and H. Bandō, *Prog. Theor. Phys.* **73**, 841 (1985).
- [4] J. F. Dubach, *Nucl. Phys.* **A450**, 71c (1986).
- [5] A. Ramos and C. Bennhold, *Nucl. Phys.* **A585**, 375c (1995); A. Ramos and C. Bennhold, *ibid.* **A577**, 287c (1994).
- [6] M. Ericson, *Nucl. Phys.* **A547**, 127c (1992); W. M. Alberico, A. De Pace, M. Ericson, and A. Molinari, *Phys. Lett. B* **256**, 134 (1991).
- [7] R. Grace *et al.*, *Phys. Rev. Lett.* **55**, 1055 (1985).
- [8] J. J. Szymanski *et al.*, *Phys. Rev. C* **43**, 849 (1991).
- [9] H. Ejiri *et al.*, KEK Proposal No. E160, Osaka University Laboratory of Nuclear Studies (OULNS) 89-1, 1989.
- [10] S. Ajimura *et al.*, *Phys. Lett. B* **282**, 293 (1992); *Phys. Rev. Lett.* **68**, 2137 (1992).
- [11] A. Yamamoto *et al.*, KEK Report No. 81-13, 1981.
- [12] M. Akei *et al.*, *Nucl. Instrum. Methods Phys. Res. Sect. A* **283**, 46 (1989); *Nucl. Phys.* **A534**, 478 (1991).
- [13] L. Lee *et al.*, *Nucl. Instrum. Methods Phys. Res. Sect. A* **372**, 287 (1993).
- [14] H. C. Chiang and J. Hüfner, *Nucl. Phys.* **A352**, 442 (1981).
- [15] T. Motoba, H. Bandō, R. Wünsch, and J. Žofka, *Phys. Rev. C* **38**, 1322 (1988).
- [16] T. Hasegawa *et al.*, *Phys. Rev. Lett.* **74**, 224 (1995).
- [17] M. Juric *et al.*, *Nucl. Phys.* **B47**, 36 (1972); W. Bruckner *et al.*, *Phys. Lett.* **55B**, 107 (1975); R. Bertini *et al.*, *Nucl. Phys.* **A360**, 315 (1981); R. E. Chrien *et al.*, *Phys. Lett.* **89B**, 31 (1979); C. Milner *et al.*, *Phys. Rev. Lett.* **54**, 1237 (1985); R. Chrien, in *LAMPF Workshop on (π, K) Physics*, edited by B. F. Gibson, W. R. Gibbs, and M. B. Johnson, AIP Conf. Proc. No. 224 (AIP, New York, 1991), p. 28.
- [18] K. Itonaga, T. Motoba, O. Richter, M. Sotona, and J. Žofka, in *Proceedings of the 5th International Symposium on Mesons and Light Nuclei*, Prague, 1991 [*Few-Body Systems Suppl.* **5**, 372 (1992)]; (private communication); see also *Phys. Rev. C* **49**, 1045 (1994).
- [19] T. Kishimoto *et al.*, *Phys. Rev. C* **51**, 2233 (1995).
- [20] A. Sakaguchi *et al.*, *Phys. Rev. C* **43**, 73 (1991).
- [21] A. Montwill *et al.*, *Nucl. Phys.* **A234**, 413 (1974).
- [22] T. Motoba, K. Itonaga, and H. Bandō, *Nucl. Phys.* **A489**, 683 (1988).
- [23] L. K. Mangotra *et al.*, *Nuovo Cimento A* **13**, 826 (1973).
- [24] C.-Y. Cheung, D. P. Heddle, and L. S. Kisslinger, *Phys. Rev. C* **27**, 335 (1983); D. P. Heddle and L. S. Kisslinger, *ibid.* **33**, 608 (1986).
- [25] A. Ramos, C. Bennhold, E. van Meijgaard, and B. K. Jennings, *Nucl. Phys.* **A554**, 703 (1992); A. Ramos, C. Bennhold, E. van Meijgaard, and B. K. Jennings, *Phys. Lett. B* **264**, 233 (1991); A. Parreño, A. Ramos, and E. Oset, *Phys. Rev. C* **51**, 2477 (1995).
- [26] A. Ramos, E. Oset, and L. L. Salcedo, *Phys. Rev. C* **50**, 2314 (1994); A. Ramos and C. Bennhold, *Nucl. Phys.* **A585**, 129c (1995).
- [27] J. J. H. Menet, E. E. Gross, J. J. Malanify, and A. Zucker, *Phys. Rev. C* **4**, 1114 (1971).
- [28] H. Ejiri, T. Fukuda, T. Shibata, H. Bandō, and K.-I. Kubo, *Phys. Rev. C* **36**, 1435 (1987).
- [29] H. Bandō, T. Motoba, M. Sotona, and J. Žofka, *Phys. Rev. C* **39**, 587 (1989).
- [30] F. Ajzenberg-Selove, *Nucl. Phys.* **A490**, 1 (1988); **A506**, 1 (1990).
- [31] M. Juric *et al.*, *Nucl. Phys.* **B52**, 1 (1973).
- [32] W. Bruckner *et al.*, *Phys. Lett.* **79B**, 157 (1978).
- [33] H. Piekarczyk *et al.*, *Phys. Rev. Lett.* **47**, 1106 (1981).
- [34] E. H. Auerbach *et al.*, *Phys. Rev. Lett.* **47**, 1110 (1981).